Solitary Wave Benchmarks in Magma Dynamics

G. Simpson*
Department of Mathematics,
University of Toronto

M. Spiegelman†
Department of Applied Physics & Applied Mathematics,
Department of Earth & Environmental Sciences,
Columbia University

December 20, 2010

Abstract

We present a model problem for benchmarking codes that investigate magma migration in the Earth's interior. This system retains the essential features of more sophisticated models, yet has the advantage of possessing solitary wave solutions. The existence of such exact solutions to the nonlinear problem make it an excellent benchmark problem for combinations of solver algorithms. In this work, we explore a novel algorithm for computing high quality approximations of the solitary waves in 1-,2- and 3 dimensions and use them to benchmark a semi-Lagrangian Crank-Nicholson scheme for a finite element discretization of the time dependent problem.

1 Introduction

Benchmark problems are of great utility for verifying and comparing numerical algorithms, and exact solutions play an important role in constructing such benchmarks. Unfortunately, exact solutions may be difficult, or impossible, to construct for nonlinear problems. In this work, we formulate a benchmark problem for the simplest non-linear model of magma migration, and explore algorithms for constructing the exact solutions and simulating the system.

On the viscous time scale, many processes in the solid Earth, including mantle convection, magma migration, and crustal deformation, occur at such low Reynolds numbers that inertial terms can be neglected. These

*simpson@math.toronto.edu
†mspieg@ldeo.columbia.edu

quasi-static systems generically take the form

$$\partial_t \psi + \nabla \cdot (\psi \mathbf{v}) = \text{sources and sinks of } \psi \tag{1a}$$

$$\nabla \cdot \sigma(\mathbf{v}; \psi) = \text{body forces on the medium} \tag{1b}$$

where ψ is some material parameter, such as temperature, fluid fraction or chemical concentration, which influence constitutive relations such as permeability or rheology of the medium. Though (1a) is written to suggest a hyperbolic nature, it may of course be parabolic, with diffusive terms appearing as sinks. All time dependence comes from the first equation, (1a), which affects the velocity field through the elliptic problem (1b), which then advects the scalar fields. This coupling introduces its own set of scientific computing challenges; there is a simultaneous need for a robust, fast, elliptic solver and an efficient time stepping algorithm.

1.1 A Reduced Model for Magma Migration

An important example of a coupled hyperbolic-elliptic systems in Earth science is the PDE's governing the flow of a low viscosity fluid in a viscously deformable porous matrix which has been used to model the flow of partially molten rock (magma) in the Earth's interior. Beginning with the primitive equations first formulated in [15], one can, after many simplifications, arrive at the system:

$$\phi_t = \phi^m \mathcal{P}, \tag{2a}$$

$$\left[\phi^m - \nabla \cdot (\phi^n \nabla)\right] \mathcal{P} = -\nabla \cdot \phi^n \mathbf{e}_d. \tag{2b}$$

In the above equations: *(i)* ϕ is porosity, or volume fraction of melt; *(ii)* $\mathcal{P}$ is the "compaction pressure", produced by volumetric deformation of the viscously deformable rock matrix. *(iii)* $\mathbf{e}_d$ is the unit vector in coordinate d associated with the direction of gravity.

The dimensionless system (2) has been scaled as follows. Porosity is scaled to a reference value $\phi_0 \sim 0.1 - 1\%$ and distance to the *compaction length*, an intrinsic length scale of the primitive system [15]. The compaction length depends on porosity, but we scale to δ_0, the compaction length at the reference porosity. All computations here are performed with respect to the dimensionless equations, however, we will often refer to lengths in terms of multiples of the reference compaction length δ_0.

The two exponents in (2), n and m, are related to the permeability and bulk viscosity of the partially molten medium. The permeability is often modeled as $K \sim \phi^n$, with $n \sim 2 - 3$. The bulk viscosity takes the form $\zeta \sim \phi^{-m}$ with $m \sim 0 - 1$, though most studies have taken either $m = 0$ or $m = 1$.

The system (2), as written, is more amenable to adding additional physics such as solid advection or melting. However, it can also be formulated as a single equation, together with a far field boundary condition as:

$$\partial_t \phi + \nabla \cdot (\phi^n \mathbf{e}_d) - \nabla \cdot \left[\phi^n \nabla \left(\phi^{-m} \partial_t \phi\right)\right] = 0, \quad \lim_{|\mathbf{x}| \to \infty} \phi(\mathbf{x}, t) = 1. \tag{3}$$

Equation (3) is a nonlinear dispersive wave equation for the evolution of porosity ϕ. Derivations from primitive equations for conservation of mass, momentum, and energy are given in [7, 18, 23].

The important feature of (3) is that it possesses *solitary wave* solutions, localized states which propagate in space at a fixed speed without changing shape. Such solutions are good for benchmarking as one need only check the distortion of the transported waveform. Indeed, in a frame moving with the solitary wave, the solution will appear constant. Numerical studies of the equation and its solitary waves have been performed in one [7, 18], two [19], and three [33] dimensions. Recent work [20–22] has shown the well-posedness of (3) and the stability of its solitary waves in dimension $d = 1$.

We demonstrate:

1. A novel algorithm for computing the solitary waves in all dimensions. This algorithm solves a time independent equation, using the Cardinal Whittaker sinc function which provide better than polynomial accuracy,
2. A semi-Lagrangian Crank-Nicolson algorithm for a finite element discretization of (2), as one algorithm for the benchmarking.

An outline of this paper is as follows. In section 2 we review some properties of the solitary waves. We then discuss the sinc collocation method in section 3.1, and how it can be implemented for these equations. Then, in section 4, we demonstrate the algorithm with convergence results. Section 5 explains the time stepping algorithm and its performance. We offer some remarks and comments in section 6.

2 Solitary Wave Solutions

The solitary wave solutions of (3) are exponentially decaying, radially symmetric humps in excess of $\phi = 1$, traveling in the x_d direction at a fixed speed. They are akin to the soliton solutions of the Zakharov-Kuznetsov equation, [34], found in plasma physics.

Making the ansatz

$$\phi(\mathbf{x}, t) = \phi_c\left(\sqrt{\sum_{j=1}^{d-1} x_j^2 + (x_d - ct)^2}\right) = \phi_c(r), \tag{4}$$

the solitary waves solve the third order equation

$$0 = \begin{cases} -c\phi_c' + (\phi_c^n)' + \dfrac{c}{1-m}\left(\phi_c^n(\phi_c^{1-m})''\right)' \\ \qquad + \dfrac{c(d-1)}{1-m}\phi_c^n\left(\dfrac{1}{r}(\phi_c^{1-m})'\right)' & m \neq 1 \\ -c\phi_c' + (\phi_c^n)' + c\left(\phi_c^n(\log\phi_c)''\right)' \\ \qquad + c(d-1)\phi_c^n\left(\dfrac{1}{r}(\log\phi_c)'\right)' & m = 1 \end{cases} \tag{5}$$

with the boundary conditions

$$\phi_c'(0) = 0 \tag{6a}$$

$$\lim_{r\to\infty} \phi_c(r) = 1 \tag{6b}$$

Derivatives are taken with respect to r.

The existence of solitary wave solutions was proven by a phase plane argument in dimension one. Further smoothness properties were stated in [21] as part of the stability analysis. The formal existence of solitary wave solutions in higher dimensions is an open problem, though it is expected. Throughout this work, we assume that smooth, monotonically decaying, solutions exist. A consequence of this is that all odd derivatives vanish at the origin.

In one dimension, (5) can always be integrated up twice, reducing the problem to quadrature. For example, in the case $n = 3$ and $m = 0$, after one integration we have

$$-c(\phi_c - 1) + \phi_c^3 - 1 + c\phi_c^3\phi_c'' = 0 \tag{7}$$

Two more integrations give the implicit expression

$$r^2 = \left(A + \frac{1}{2}\right)\left[-2\sqrt{A-\phi_c} + \frac{1}{\sqrt{A-1}}\log\left(\frac{\sqrt{A-1}-\sqrt{A-\phi_c}}{\sqrt{A-1}+\sqrt{A-\phi_c}},\right)\right]^2 \tag{8}$$

where $A = (c-1)/2$ is the amplitude.

2.1 Reformulation by Even Extension

For higher dimensions, such integrations of (5) are not possible and we resort to numerical approximation. First, (5) is rewritten to make it more amenable to computation. Integrating from r to ∞ yields the integro-differential equation

$$0 = \begin{cases} -c(\phi_c - 1) + (\phi_c^n - 1) + \dfrac{c}{1-m}\left(\phi_c^n(\phi_c^{1-m})''\right) & \\ \qquad - \dfrac{c(d-1)}{1-m}\displaystyle\int_r^\infty \phi_c^n\left(\frac{1}{r}(\phi_c^{1-m})'\right)' dr & m \neq 1 \\ -c(\phi_c - 1) + (\phi_c^n - 1) + c\left(\phi_c^n(\log\phi_c)''\right) & \\ \qquad - c(d-1)\displaystyle\int_r^\infty \phi_c^n\left(\frac{1}{r}(\log\phi_c)'\right)' dr & m = 1 \end{cases} \tag{9}$$

Barcilon & Lovera [6], also solved (9) numerically using a shooting method. However, this approach was unstable for moderate amplitude waves and only considered the parameters $n = 3$, $m = 0$. The sinc-collocation method we use here appears to be robust for a wide range of wave parameters in all dimensions.

The sinc-collocation method, however, does not apply directly to problems posed on the semi-axis, $(0, \infty)$. The problem must be altered to live on all of $(-\infty, \infty)$. Let

$$\tilde{\phi}_c(x) = \phi_c(|x|) \tag{10}$$

be the even extension of ϕ_c to the whole real line. Dropping the ˜'s, ϕ_c solves

$$0 = \begin{cases} -c(\phi_c - 1) + \phi_c^n - 1 + \dfrac{c}{1-m}\left(\phi^n(\phi_c^{1-m})''\right) \\ \qquad\qquad + \dfrac{c(d-1)}{1-m}\displaystyle\int_{-\infty}^{x} \phi_c^n \left(\frac{1}{x}(\phi_c^{1-m})'\right)' dx & m \neq 1 \\ -c(\phi_c - 1) + \phi_c^n - 1 + c\left(\phi_c^n(\log\phi_c)''\right) \\ \qquad\qquad + c(d-1)\displaystyle\int_{-\infty}^{x} \phi_c^n \left(\frac{1}{x}(\log\phi_c)'\right)' dx & m = 1 \end{cases} \tag{11}$$

We discretize and solve (11) using the sinc-collocation method, described in Section 3.1.

3 Collocation & Continuation

Equation (11) is a nonlinear integro-differential equation posed on an unbounded domain. We employ a method, sinc-collocation, that respects these features. The sinc spectral method is thoroughly formulated and explained in [12, 27–29] and briefly in Appendix A. In the sinc discretization, the problem remains posed on $\mathbb{R}$ and the boundary conditions, that the solution vanish at $\pm\infty$, are naturally incorporated. This method has been applied to a variety of differential equations; see the above references. It has been used to compute solitary waves in the early work [13] and more recently in [14]. It was also used to study a time dependent problem, KdV, in [2].

Collocation insists the equation be satisfied at the nodes of the mesh. This is in contrast to a Galerkin formulation, which would have us discretely orthogonalize the residual against some family of functions. Collocation can be interpreted as discretely solving the classical form of the equation, while Galerkin discretely solves the weak form. Moshen & El-Gamel found collocation to be superior for certain problems, [16].

This discretization will lead to a nonlinear system of algebraic equations, requiring a good initial guess for the solver. Our strategy for constructing such a solution is to take the $d = 1$ solution and then perform numerical continuation in dimension, up to the desired value. Constructing the $d = 1$ solution is also done by continuation, using an asymptotic approximation in the small amplitude, $c \sim n$, state; continuation is performed in c to its desired value.

3.1 Sinc Discretization

Given a function $u : \mathbb{R} \to \mathbb{R}$, u is approximated using a superposition of shifted and scaled sinc functions:

$$C_{M,N}(u,h)(x) \equiv \sum_{k=-M}^{N} u_k \mathrm{sinc}\left(\frac{x - x_k}{h}\right) = \sum_{k=-M}^{N} u_k S(k,h)(x), \tag{12}$$

where $x_k = kh$ for $k = -M, \ldots, N$ are the *nodes* and $h > 0$. There are *three* parameters in this discretization, h, M, and N, determining the

number and spacing of the lattice points. This is common to numerical methods posed on unbounded domains, [9].

A useful and important feature of this spectral method is that the $S(k,h)$ functions act like discrete delta functions,

$$C_{M,N}(u,h)(x_k) = u_k. \tag{13}$$

For sufficiently smooth functions, the convergence of this approximation is rapid both in practice and theoretically. See Theorem A.2 in Appendix A for a statement on convergence.

Since the solution is even, we may take $N = M$; we write

$$C_M(u,h)(x) \equiv C_{M,M}(u,h)(x). \tag{14}$$

We further reduce the number of free parameters down to just M, by slaving h to M as

$$h = \pi\sqrt{\frac{1}{2\gamma M}}, \quad \gamma = \sqrt{1-\frac{n}{c}} \tag{15}$$

The motivation for this choice is discussed in Appendix A. It is closely connected to the theory of the sinc method, and the asymptotic decay properties of both $\phi_c - 1$ and its Fourier transform.

Letting $u_c = \phi_c - 1$, the solitary wave with the asymptotic state subtracted off, we formulate (11) as a nonlinear collocation problem at the nodes $\{x_k\}$:

$$0 = \begin{cases} \begin{aligned} &-cC_M(u_c,h)(x_k) + (C_M(u_c,h)(x_k)+1)^n - 1 \\ &+\frac{c}{1-m}\left(C_M(u_c,h)(x_k)+1\right)^n \frac{d^2}{dx^2}\left(C_M(u_c,h)(x_k)\right)^{1-m} \\ &+\frac{c(d-1)}{m-1}\int_{x_k}^{\infty}(C_M(u_c,h)(x)+1)^n x\frac{d}{dx}\left\{\frac{1}{x}\frac{d}{dx}\left[\left(C_M(u_c,h)(x)\right)^{1-m}\right]\right\}dx. \end{aligned} & m \neq 1 \\ \begin{aligned} &-cC_M(u_c,h)(x_k) + (C_M(u_c,h)(x_k)+1)^n - 1 \\ &+c\left(C_M(u_c,h)(x_k)+1\right)^n \frac{d^2}{dx^2}\left(\log C_M(u_c,h)(x_k)\right) \\ &+c(d-1)\int_{x_k}^{\infty}(C_M(u_c,h)(x)+1)^n x\frac{d}{dx}\left\{\frac{1}{x}\frac{d}{dx}\left[\log C_M(u_c,h)(x)\right]\right\}dx. \end{aligned} & m = 1 \end{cases} \tag{16}$$

From here on we suppress the subscripts c in u_c and ϕ_c.

Let $\mathbf{u}$ be the column vector associated with the sinc discretization of u, at the collocation points $\{x_k\}$,

$$C_M(u,h)(x_k) \mapsto \mathbf{u} = \begin{pmatrix} u_{-M} & u_{-M+1} & \dots & u_M \end{pmatrix}^T. \tag{17}$$

Associated with $\mathbf{u}$ is $\boldsymbol{\phi} = \mathbf{u} + \mathbf{1}$.

We now define a series of matrices that operate on $\mathbf{u}$. The derivatives of sinc approximated functions are given by:

$$D^{(l)}_{jk} = \frac{d^l}{dx^l} S(j,h)(x)|_{x=x_k} \tag{18}$$

Explicitly,

$$D^{(1)}_{jk} = \begin{cases} 0 & j = k \\ \frac{1}{h}\frac{(-1)^{k-j}}{k-j} & j \neq k \end{cases} \tag{19a}$$

$$D^{(2)}_{jk} = \begin{cases} \frac{1}{h^2}\frac{-\pi^2}{3} & j = k \\ \frac{1}{h^2}\frac{-2(-1)^{k-j}}{(k-j)^2} & j \neq k \end{cases} \tag{19b}$$

The integration matrix is

$$D^{(-1)}_{jk} = \frac{h}{2} + \frac{h}{\pi}\mathrm{Si}(\pi(j-k)) \tag{20}$$

where Si is the sine-integral function,

$$\mathrm{Si}(x) \equiv \int_0^x \frac{\sin(t)}{t} dt. \tag{21}$$

Being singular, the $\frac{1}{x}\frac{d}{dx}$ operator must be treated carefully. For smooth even functions ($u'(0) = 0$), it is well defined. Taking limits of the sinc approximation of an even function ($u_{-k} = u_k$),

$$\lim_{x\to 0} \frac{1}{x}\partial_x u_0 S(0,h)(x) = -\frac{\pi^2}{3h^2}u_0, \tag{22}$$

$$\lim_{x\to 0} \frac{1}{x}\left(\partial_x u_k S(k,h)(x) + \partial_x u_{-k} S(-k,h)(x)\right) = -4\frac{(-1)^k}{h^2k^2}u_k. \tag{23}$$

The matrix $\tilde{D}^{(1)}$ approximating $\frac{1}{x}\frac{d}{dx}$ is defined as:

$$\tilde{D}^{(1)}_{jk} = \begin{cases} \frac{1}{x_j} D^{(1)}_{jk} & j \neq 0, \\ -\frac{2(-1)^k}{h^2k^2} & j = 0, k \neq 0, \\ \frac{-\pi^2}{3h^2} & j = k = 0. \end{cases} \tag{24}$$

With these matrices, the discretization of (11) is equivalent to the nonlinear algebraic system

$$\mathbf{F}(\mathbf{u}) = \begin{cases} -c\mathbf{u} + \boldsymbol{\phi}^n - \mathbf{1} + \dfrac{c}{1-m}\boldsymbol{\phi}^n D^{(2)}(\boldsymbol{\phi}^{1-m} - \mathbf{1}) & \\ \qquad + \dfrac{c(d-1)}{1-m} D^{(-1)}(\boldsymbol{\phi})^n D^{(1)}\tilde{D}^{(1)}(\boldsymbol{\phi}^{1-m} - \mathbf{1}) & m \neq 1 \\ -c\mathbf{u} + \boldsymbol{\phi}^n - \mathbf{1} + c\boldsymbol{\phi}^n D^{(2)} \log \boldsymbol{\phi} & \\ \qquad + c(d-1) D^{(-1)} \boldsymbol{\phi}^n D^{(1)} \tilde{D}^{(1)} \log \boldsymbol{\phi} & m = 1 \end{cases} \tag{25}$$

where $\mathbf{1}$ is a vector of size $2M+1$ with 1's in all entries. Nonlinear terms should be interpreted as component-wise operations on the vectors.

3.2 Initial Guesses and Numerical Continuation

To solve (25), one needs a good initial guess for $\mathbf{u}$. For dimension one, an excellent guess is available. Integrating (5) reduces the equation to first order, which can be solved by quadrature and root finding. Sometimes it is even possible to obtain implicit solution, as in (8). This is not possible for $d > 1$, nor is it always desirable to work out the quadrature formulas. Thus, for a given c and d, we proceed in two sequential steps:

- For $d = 1$, perform numerical continuation in c, from a value of $c \sim n$, up to the desired value.
- For $d > 1$, apply the continuation in c to construct the solution in $d = 1$, then perform numerical condition in d, up to the desired dimension.

Other continuation paths in (c, d) parameter space are possible, but this proved to be robust. Throughout the two continuation sequences, we keep the nonlinearities, n and m, fixed.

3.2.1 Continuation in c

In [32], the authors observed that in the limit of small amplitude disturbances of the reference state, (3) was, to leading order, governed by the Korteweg - de Vries equation. Generalizing this observation in [21], let

$$\gamma = \sqrt{1 - \frac{n}{c}}, \tag{26a}$$

$$\phi_c(x_1 - ct) = 1 + \frac{\gamma^2}{n-1} U(\gamma(x_1 - ct)). \tag{26b}$$

Then U solves the equation

$$-U + \frac{1}{2}U^2 + \partial_\xi^2 U = \mathrm{O}(\gamma^2), \tag{27}$$

and small amplitude solitons, where $0 < \gamma \ll 1$, are approximately

$$\phi_c(r) = 1 + \frac{3\gamma^2}{n-1} \mathrm{sech}^2\left(\frac{1}{2}\gamma r\right) + \mathrm{O}(\gamma^4). \tag{28}$$

Given the desired value of c, we partition $(n, c]$ into P points

$$n < c_1 < c_2 < \ldots < c_P = c \tag{29}$$

we iteratively solve

$$\mathbf{G}(\mathbf{u}; c) = \begin{cases} -c\mathbf{u} + \boldsymbol{\phi}^n - \mathbf{1} + \frac{c}{1-m}\boldsymbol{\phi}^n D^{(2)}(\boldsymbol{\phi}^{1-m} - \mathbf{1}) & m \neq 1 \\ -c\mathbf{u} + \boldsymbol{\phi}^n - \mathbf{1} + \frac{c}{1-m}\boldsymbol{\phi}^n D^{(2)} \log \boldsymbol{\phi} & m = 1 \end{cases} \tag{30}$$

using $\mathbf{u}^{(j)}$ as the initial guess for

$$\mathbf{G}(\mathbf{u}^{(j+1)}; c_{j+1}) = \mathbf{0} \tag{31}$$

The $\mathbf{u}^{(1)}$ guess is given by (28). We have successfully solved with $P = \mathrm{O}\left(10\frac{c}{n}\right)$, though this could likely be refined with more sophisticated continuation algorithms.

3.2.2 Continuation in d

For $d > 1$ we solve by numerical continuation in dimension by making d a parameter:

$$\mathbf{H}(\mathbf{u}; d) = \begin{cases} -c\mathbf{u} + \boldsymbol{\phi}^n - \mathbf{1} + \dfrac{c}{1-m}\boldsymbol{\phi}^n D^{(2)}(\boldsymbol{\phi}^{1-m} - \mathbf{1}) \\ \qquad + \dfrac{c(d-1)}{1-m} D^{(-1)}\boldsymbol{\phi}^n D^{(1)}\tilde{D}^{(1)}(\boldsymbol{\phi}^{1-m} - \mathbf{1}) & m \neq 1 \\ -c\mathbf{u} + \boldsymbol{\phi}^n - \mathbf{1} + c\boldsymbol{\phi}^n D^{(2)} \log \boldsymbol{\phi} \\ \qquad + c(d-1)D^{(-1)}\boldsymbol{\phi}^n D^{(1)}\tilde{D}^{(1)} \log \boldsymbol{\phi} & m = 1 \end{cases} \tag{32}$$

Given the dimension d for which we desire a solution, we partition $[1, d]$ into

$$1 = d_0 < d_1 < d_2 < \ldots d_P = d. \tag{33}$$

Then, assuming we have solved

$$\mathbf{H}(\mathbf{u}^{(j)}; d_j) = \mathbf{0},$$

$\mathbf{u}^{(j)}$ becomes the initial guess for d_{j+1}. P, the partition size of $[1, d]$, need not be that large. $P = \mathrm{O}(10d)$ appears sufficient. As with continuation in c, more sophisticated continuation algorithms might improve this.

3.3 System Size Reductions

The even symmetry can be exploited to reduce the size of the algebraic system. Since $u_{-k} = u_k$, we need only track u_k, $k = 0, 1, \ldots M$. The symmetry is imposed on (25) by the following manipulations on a discretized operator, A. Since only the last $M + 1$ rows are required, we only retain A_{ij} for $i = M + 1, \ldots 2M + 1$. Next, we add or subtract the columns A_{ij}, $j = 1, \ldots M$ onto the columns $j = 2M + 1, \ldots M + 2$. For even/odd symmetry preserving operations, $\frac{d^2}{dx^2}$ and $\frac{1}{x}\frac{d}{dx}$, we add. For even/odd symmetry reversing operations, $\frac{d}{dx}$ and $\int_{-\infty}^{x}$, we subtract. This reduces the system to $M + 1$ points.

4 Example Solitary Wave Computations

We implemented our algorithm using NumPy/SciPy. This has the advantages of being open source and easily integrating with our time dependent algorithms through Python. The codes for computing the sinc-collocation matrices were motivated by the MATLAB codes discussed in [31]. For solving the nonlinear system, we used the `fsolve` routine in SciPy, which is a Python wrapped MINPACK routine.

4.1 Solitary Wave Forms

As a first example of our results, we compute a collection of solitary waves for different parameter values and dimensions. These wave forms are pictured in Figure 1. The amplitudes and width of the waves tend to increase with dimension. We have not observed a choice of (c, n, m) for

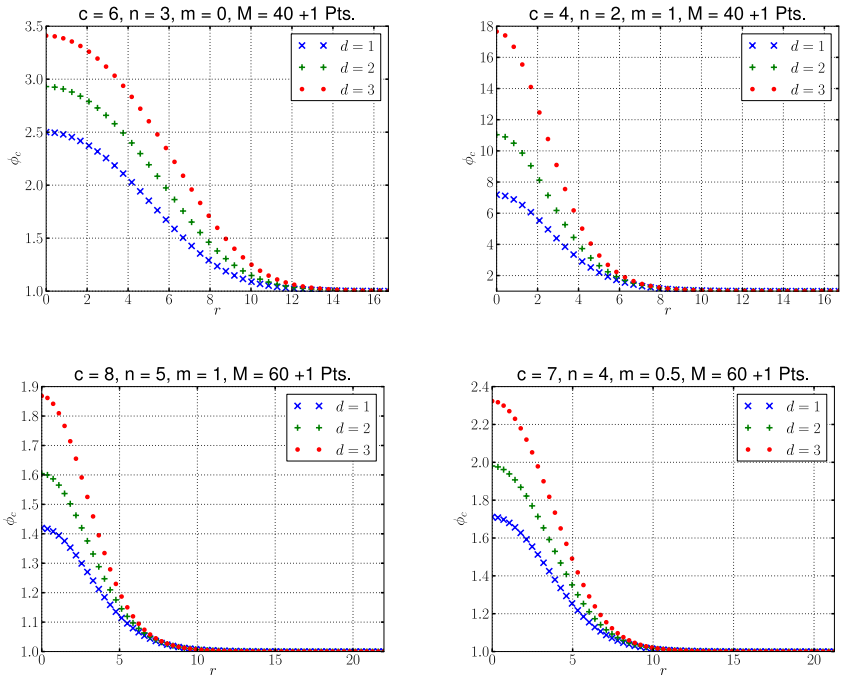

Figure 1: Examples of computed solitary waves with different values of c, n, m, and M.

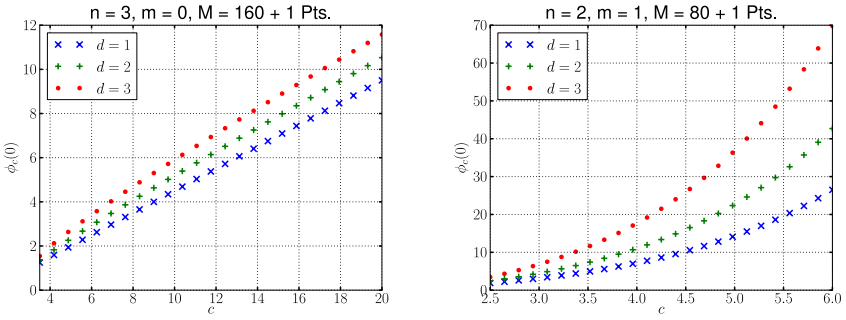

Figure 2: Dispersion relations between c and solitary wave amplitude.

which this does not happen. This observation was previously noted in [33] for the $n = 3$, $m = 0$ case.

We can further consider this relationship between dimension and amplitude by plotting "dispersion relations" between the parameter c, and the amplitude of the associated solitary wave. See Figure 2. The $n = 2$, $m = 1$ case has a much more nonlinear dispersion relation than $n = 3$, $m = 0$ case.

4.2 Convergence

Not only does the sinc-collocation approach work, but it also converges quite rapidly to the desired solution. We now present some benchmarks on the convergence of the amplitudes of the solitary waves in different dimensions, for different choices of (c, n, m). We focus on comparing the amplitudes $(\phi_c(0))$. Other points are more difficult to compare as the grids change with M. The results are given in Table 4.2.

5 Time Dependent Simulations

Spectrally accurate solitary wave profiles are extremely useful as initial conditions for benchmarking and exploring numerical solutions of the full space time PDE's. For example, Figure 3 shows a solution for an off-center collision of two 2-D solitary waves with speeds $c = 5$ and $c = 7$ initialized with two sinc-collocation solutions. This calculation is done in a moving frame translating at the mean velocity of the two waves which allows long runs in limited numerical domains. More specifically we solve a variation of the coupled hyberbolic-elliptic problem, (2) for porosity ϕ and compaction pressure $\mathcal{P}$ [10]:

$$\frac{D\phi}{Dt} = \phi^m \mathcal{P} \tag{34a}$$

$$[-\nabla \cdot \phi^n \nabla + \phi^m]\,\mathcal{P} = -\nabla \cdot \phi^n \mathbf{e}_d \tag{34b}$$

Table 1: Convergence of the solitary wave amplitude for three difference c, n and m configurations.

(a) $c = 4$, $n = 3$, $m = 0$

M	$d = 1$	$d = 2$	$d = 3$
20	1.50021353765	1.70417661440	1.96849289246
40	1.50000080060	1.70608902282	1.97466312561
60	1.50000000989	1.70617046612	1.97486670209
80	1.50000000023	1.70617690685	1.97488105982
100	1.50000000001	1.70617767812	1.97488264950
200	1.50000000000	1.70617782834	1.97488293768
400	1.50000000000	1.70617782848	1.97488293789
800	1.50000000000	1.70617782848	1.97488293789

(b) $c = 5$, $n = 2$, $m = 1$

M	$d = 1$	$d = 2$	$d = 3$
20	14.3312283238	22.5954364016	36.4572095987
40	14.2972695906	22.6643001828	36.8255142055
60	14.2972368619	22.6667057152	36.8329976531
80	14.2972367260	22.6668188493	36.8333101100
100	14.2972367248	22.666827544	36.8333323307
200	14.2972367248	22.6668286095	36.8333348778
400	14.2972367248	22.6668286096	36.8333348781
800	14.2972367247	22.6668286095	36.8333348777

(c) $c = 6$, $n = 4$, $m = .5$

M	$d = 1$	$d = 2$	$d = 3$
20	1.47945862654	1.67961148369	1.94941026371
40	1.47938232695	1.68059282799	1.95217168937
60	1.47938214568	1.68062352158	1.95223978609
80	1.47938214411	1.68062557559	1.95224385885
100	1.47938214408	1.68062579033	1.95224425280
200	1.47938214408	1.68062582653	1.95224431473
400	1.47938214408	1.68062582655	1.95224431476
800	1.47938214408	1.68062582655	1.95224431476

where $\mathbf{e}_d$ is the unit vector in the direction of gravity and

$$\frac{D\phi}{Dt} = \frac{\partial \phi}{\partial t} + \mathbf{v} \cdot \nabla \phi$$

is the material derivative in a frame moving at speed $\mathbf{v}$ (which we assume is constant for these problems, but can vary in space and time for more general magma dynamics problems).

Given any numerical method for solving (34), the sinc solitary wave solutions provide a straightforward benchmark problem: use a high resolution ($M = 400$) solitary wave as an initial condition and solve. A perfect scheme would have the wave propagate at speed c with no change in shape; anything else is numerical error.

5.1 Numerical Methods

System (34) has previously been solved by finite difference and finite volume methods with explicit time stepping and operator splitting [33, e.g.]. Here we describe and benchmark more recent implicit finite element codes with semi-Lagrangian/Crank-Nicolson time stepping for the advection terms. Specifically, we solve the non-linear variational problem

$$\begin{aligned} F(\mathbf{u}) = &\int_\Omega \left[f^n \nabla v \cdot (\nabla p - \mathbf{e}_d) + v f^m p \right] dV + \int_{\partial\Omega} f^n \mathbf{e}_d \cdot d\mathbf{S} \\ &+ \int_\Omega q(f - \frac{\Delta t}{2} f^m p - g(\mathbf{x}^*)) dV = 0 \end{aligned} \tag{35}$$

for consistent porosity, f, and pressure, p, at time $t + \Delta t$. Here, $\mathbf{u} = (p, f)$ is a solution for pressure and porosity in a mixed finite element space $\mathcal{V}$ with test functions $\mathbf{v} = (v, q)$. For the problems shown here we use second order elements on triangular (2D) and tetrahedral meshes (3D) (*e.g.* $\mathcal{V} = [P2 \times P2]$). The semi-Lagrangian source function

$$g(\mathbf{x}^*) = f(\mathbf{x}^*, t) + \frac{\Delta t}{2} f(\mathbf{x}^*, t)^m p(\mathbf{x}^*, t), \tag{36}$$

depends on the porosity and pressure at the previous time step evaluated at the takeoff point of the characteristics that intersect the quadrature points at time $t + \Delta t$ [25, 26, e.g.]. For constant background advection $\mathbf{x}^* = \mathbf{x} - \mathbf{v}\Delta t$.

Equation (35) is non-linear with $F(\mathbf{u})$ being the residual for any function $\mathbf{u} \in \mathcal{V}$. We solve $F(\mathbf{u}) = 0$, using pre-conditioned Newton-Krylov methods implemented in hybrid FEniCS (http://www.fenics.org) and PETSc [3–5] codes. FEniCS is a suite of advanced, open-source software libraries and applications that allows for high-level description of weak forms using a "unified form language" (ufl) that can be translated into efficient, compilable C++ code using their form compiler FFC. In addition ufl has the capability of describing and calculating the weak form of the exact Jacobian ($J(u) = \delta F / \delta u$) by automatic functional differentiation. Given weak forms for both the residual and Jacobians, FEniCS provides routines for assembling variational forms into discrete vectors and matrices, which are used in PETSc's non-linear equation solvers (SNES). These codes are flexible and can easily compose a wide range of PDE based models and adjust

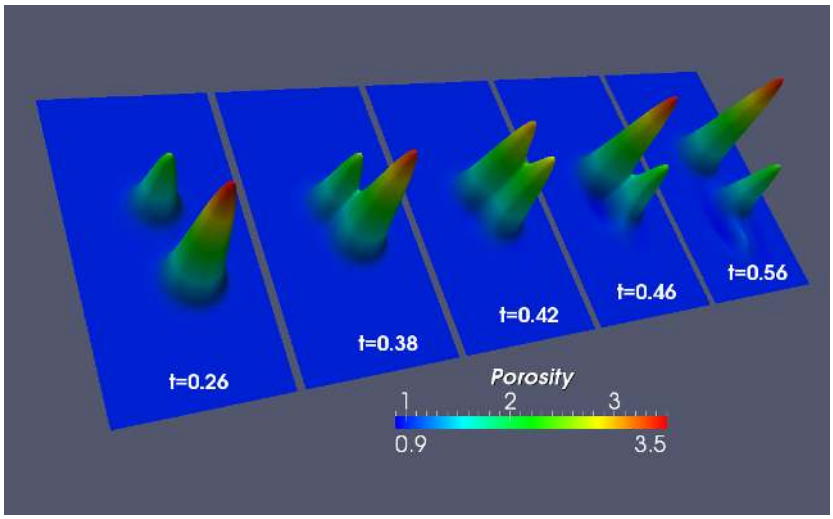

(a)

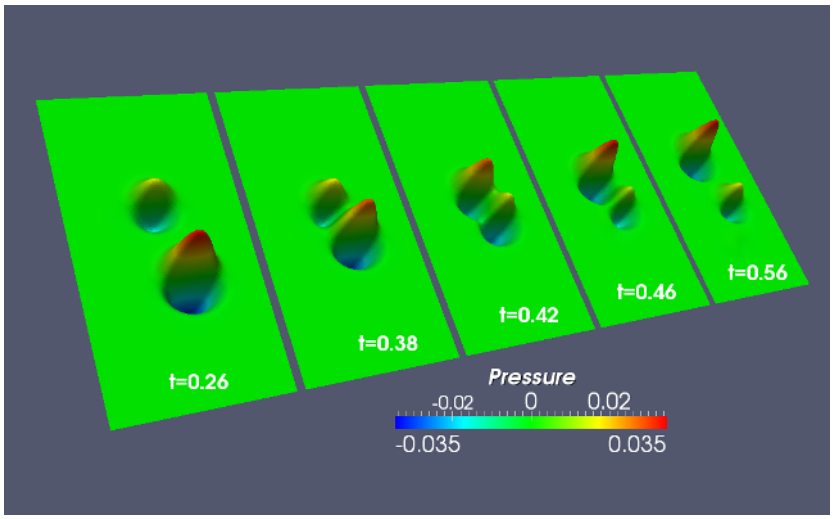

(b)

Figure 3: Figure showing the off-center collision of two solitary waves with wave-speeds $c = 7$ and $c = 5$ and material exponents $n = 3$, $m = 0$ in dimension $d = 2$. (a) Porosity. (b) Compaction Pressure. Model domain is 64×128 compaction lengths with 128×256 degrees of freedom (node spacing $h = 0.5\delta$). Courant number is 1. This model is calculated in a frame moving at the mean speed of the two waves ($V = 6$) and shows the typical non-linear phase shift interaction with some radiation loss on collision.

Table 2: Parameters for solitary wave benchmarks

n	m	c	Amplitude	Ω (compaction lengths)	$\lvert\mathcal{C}''\rvert_{\max}$
2D runs:					
3	0	5	2.33407	64×64	0.11054
3	0	10	5.18711	64×64	0.31226
2	1	2.5	2.44620	64×64	0.17679
2	1	4	11.03790	64×64	3.61868
3D runs:					
3	0	5	2.72588	$32 \times 32 \times 32$	0.12869

solver strategies at run time. We have used these codes to explore a variety of physics-based block preconditioning strategies for iterative solutions of the magma equations. Appendix B provides details of the numerical method used here. Benchmark codes are available through the Computational Infrastructure for Geodynamics, CIG, www.geodynamics.org.

5.2 Benchmark problems and results

Table 2 gives parameters for four 2-D problems and one 3-D problem. For each problem we set the background advection velocity to $\mathbf{v} = -c\mathbf{e}_d$ so that the wave appears stationary in the moving frame. Each model run is calculated on a square or cubic domain large enough so that the tails of the solitary wave are $\phi_c - 1 \lesssim 10^{-7}$, with boundary conditions $(f, p) = (1, 0)$ on the top edge and "free-flux" $(\nabla\mathcal{P} \cdot \hat{\mathbf{n}} = 0)$ on the other three sides. For each wave, we consider a series of spatial and temporal discretizations by varying the inter-node spacing $h = .25$, 0.5 and $1.0\delta_0$ where δ_0 is the compaction length in the constant porosity background. Time steps are chosen such that each wave moves a fixed multiple of a compaction length in a time-step, *i.e.* $c\Delta t/\delta_0 = 0.125$, 0.25, 0.5, 1.0 and 2.0. The Courant number is $c\Delta t/h$.

Semi-Lagrangian schemes are characteristic based and do not have a CFL stability condition. This allows for large time steps. Nevertheless, as the results here show, accuracy is degraded at large time-steps. For this problem, the most efficient and accurate runs occur at CFL = 1.

For this problem, two natural measures of error are distortion of the wave shape and disturbance of the phase speed. Given a computed solution for porosity $f(\mathbf{x}, t)$, we identify both types of errors by first minimizing the functional

$$\mathcal{E}(\boldsymbol{\delta}) \equiv \int \left(f(\mathbf{x}, t) - \boldsymbol{\phi}_c(\mathbf{x} + \boldsymbol{\delta}, t)\right)^2 d\mathbf{x} \tag{37}$$

where $\boldsymbol{\phi}_c$ is a high quality approximation of the solitary wave at time t. Though this can be done by direct minimization of the functional, it is more accurate to solve the nonlinear system

$$\langle \mathbf{f}(\mathbf{x}) - \boldsymbol{\phi}_c(\mathbf{x} + \boldsymbol{\delta}), \nabla\boldsymbol{\phi}_c(\mathbf{x} + \boldsymbol{\delta})\rangle = 0 \tag{38}$$

Numerical experimentation shows that this optimization/root finding problem reduces to a single parameter system for the vertical component

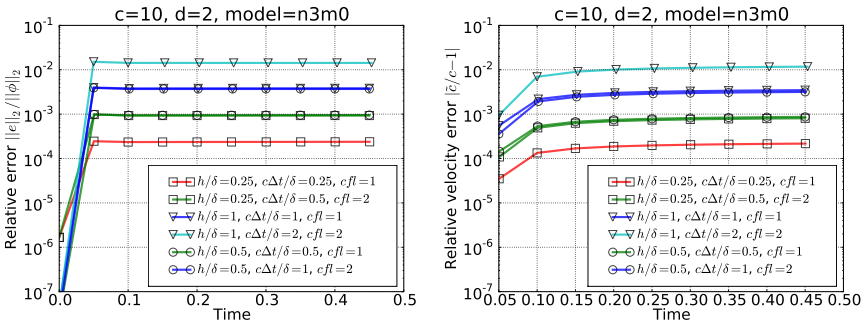

(a) (b)

Figure 4: Relative errors in (a) Shape and (b) Velocity for a 2-D, $n = 3$, $m = 0$, $c = 10$ wave as a function of time, grid spacing h/δ_0 (symbols) and time-step Δt (line color). Note, problems with the same time-step but different grid spacing overlap and have nearly identical errors. Grid spacing is the distance between nodes for quadratic elements and is relative to the compaction length in the constant porosity background. $c\Delta t/\delta_0$ gives the number of reference compaction lengths traveled in a time step. The Courant number is $c\Delta t/h$. For all runs, there is a rapid adjustment from the initial condition and then a steady evolution with little to no change in shape or velocity.

of the displacement $\boldsymbol{\delta}$ due to the symmetries of the equation. $\boldsymbol{\delta}$ measures the phase shift, from which we can find the error in the speed parameter,

$$\boldsymbol{\delta} \approx (\tilde{c} - c)t$$

where $\tilde{c}$ is the speed of the numerically perturbed solitary wave. Once we have found $\boldsymbol{\delta}$, we can directly compute the L^2 error in the approximations.

Figure 4 shows the relative shape error $\sqrt{\mathcal{E}}/||\phi_c||_2$ and relative velocity error $|\tilde{c}/c - 1|$ as a function of time for a $n = 3, m = 0, c = 10$ wave and a range of grid spacing and time steps. Similar to previous solitary wave studies [24], the initial conditions rapidly adjust to an approximate solitary wave in the discrete function space and then propagates with constant form and phase speed. An interesting feature of this algorithm, is that it appears that the errors in both shape and wave-speed depend primarily on the absolute time step Δt and not on the grid-spacing h. This can be seen in Figure 4 where runs with different grid spacing and the same time-step have nearly identical errors for problems with integer Courant number. Figure 5 shows the convergence of the same set of runs with respect to time step at the maximum run time $t = 0.45$. For all Courant numbers, the convergence is $\mathrm{O}(\Delta t^2)$, but there are discrepancies for non-integer Courant numbers. Most likely, this is due to accumulated interpolation errors at very small time steps. However, for integer CFL=$1, 2$, the error at for the same time-step is nearly identical. Figure 6 shows the same plot for all initial wave forms in Table 2 (both 2- and 3-D and integer Courant number.

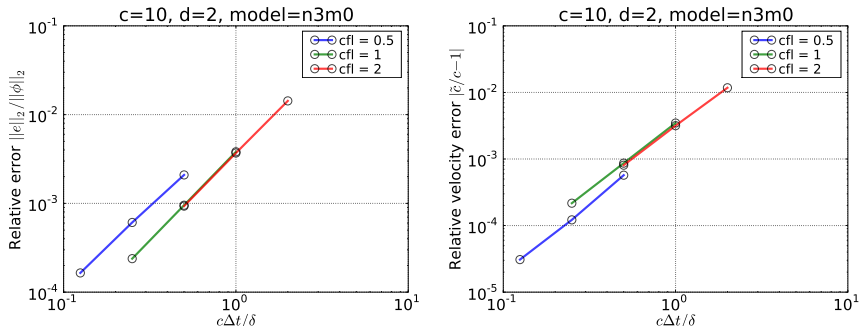

Figure 5: Convergence behavior as a function of time step at $t \sim 0.45$ for the runs shown in Fig. 4. For any given Courant number, the error shows second order convergence and runs with integer Courant number show nearly identical errors for the same time-step Δt. Runs with fractional Courant number show similar convergence but larger shape errors (and in this case smaller velocity errors) at the same time-step. For these runs highest accuracy per computational work occurs for Courant number CFL = 1 runs.

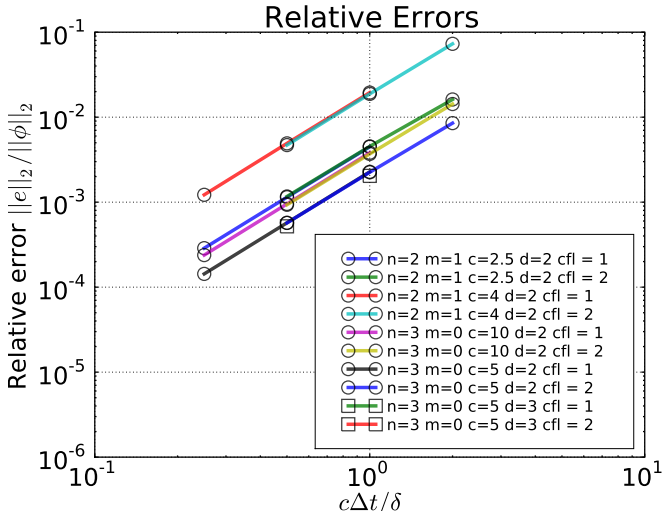

Figure 6: Convergence behavior for all runs as a function of time-step. All problems show second-order convergence with Δt and integer Courant number (and is independent of h). Relative error for all waves is $\lesssim 10^{-3}$ for grid-spacing $h = 0.25$, CFL=1.

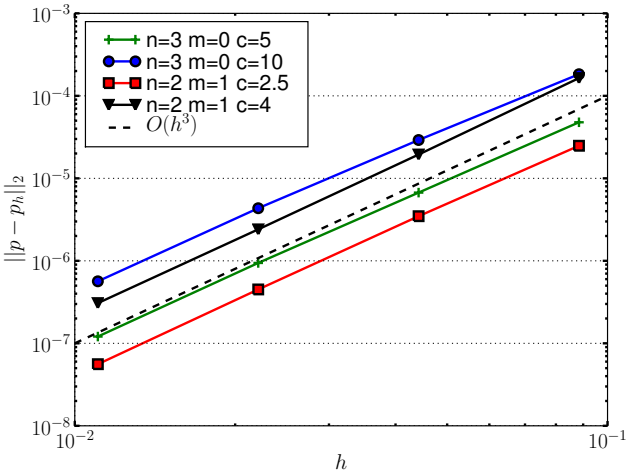

Figure 7: Convergence behavior of pressure solution with respect to grid spacing h. Figure shows the L^2 norm of the absolute error ($||p - p_h||_2$) between the discrete FEM solution with quadratic elements and the "true" solution given by an extremely high-resolution sinc-collocation solution. Dotted line shows expected convergence if $O(h^3)$.

To explain these results, we note that this algorithm has two sources of error. The first source is in the solution of the elliptic problem, (34b), for the pressure field, which depends on the grid-spacing h. Figure 7 shows that the error in pressure, given an exact porosity profile for a solitary wave $\phi = \phi_c(r)$, scales as $\mathrm{O}(h^3)$ for quadratic elements. Thus, for fine meshes, we expect that the pressure is well resolved.

The second source of error comes from the semi-Lagrangian time-stepping algorithm. Equation (34a) can be written exactly for a constant advection velocity $\mathbf{v}$ as

$$\phi(\mathbf{x}, t + \Delta t) = \phi(\mathbf{x}^*, t) + \int_t^{t+\Delta t} \mathcal{C}(\mathbf{x}^* + \mathbf{v}(\tau - t), \tau) d\tau \qquad (39)$$

where $\mathcal{C} = \phi^m \mathcal{P}$ is the "compaction rate", [23]. The final term is the line integral across the straight characteristic between point $(\mathbf{x}, t + \Delta t)$ and $(\mathbf{x}^*, t)$ where $\mathbf{x}^* = \mathbf{x} - \mathbf{v}\Delta t$.

In the special case that ϕ is a solitary wave of speed c and $\mathbf{v} = -c\mathbf{e}_d$, then the solitary waves are independent of time in this coordinate system; $\phi_c = \phi_c(x)$. If the line integral could be done exactly, then (39) reduces

to the identity:

$$\begin{aligned}
&\int_t^{t+\Delta t} \mathcal{C}(\mathbf{x}^* + \mathbf{v}(\tau - t), \tau) d\tau \\
&\quad = \int_t^{t+\Delta t} \phi_c' \left(r(\mathbf{x}^* + \mathbf{v}(\tau - t)) \right) \frac{\partial r}{\partial \tau} \left(\mathbf{x}^* + \mathbf{v}(\tau - t) \right) d\tau \\
&\quad = \int_t^{t+\Delta t} \frac{\partial}{\partial \tau} \phi_c \left(\mathbf{x}^* + \mathbf{v}(\tau - t) \right) d\tau \\
&\quad = \phi_c(r(\mathbf{x}^* + \mathbf{v}\Delta t)) - \phi_c(r(\mathbf{x}^*)) \\
&\quad = \phi_c(\mathbf{x}) - \phi_c(\mathbf{x}^*)
\end{aligned} \tag{40}$$

where $r = |\mathbf{x}|$. Clearly, this is valid for any time step Δt.

Were the integration exact, the numerical errors in the pressure field would lead us to expect a single step error of $\mathrm{O}(h^3 \Delta t)$ arising from errors in the solving the elliptic problem. Here, however, we implemented a trapezoidal rule for the integral, and expect a single-step error of order $\mathrm{O}(\Delta t^3 \max |\mathcal{C}''| + h^3 \Delta t)$ and a global error of $\mathrm{O}(\Delta t^2 \max |\mathcal{C}''| + h^3)$. Thus, for a well resolved pressure field, we expect time step errors to dominate. Table 2 lists $\max |\mathcal{C}''|$ calculated from the sinc-collocation solitary waves benchmarked here which is clearly larger for larger amplitude/faster waves, and in particular, is noticeably larger for the $n = 2$, $m = 1$ waves, in qualitative agreement with the general results shown in Figure 6.

These results indicate that a higher order time-integrator could improve the accuracy of this algorithm, at least until the spatial errors became dominant. While many approaches could be used for the special case of a single solitary wave in a co-moving frame, the challenge remains to find a high quality, but easily adaptable, time integrator/advection scheme for more general magma dynamics problems.

6 Discussion

One of the challenges of studying Eq. (3) is that it is fully nonlinear. This carries over to the solitary wave equation (5). As previously discussed, for $d > 1$, this cannot be reduced to a first integral. For other multidimensional equations, such as the Nonlinear Schrödinger (NLS) equation and the Zakharov-Kuznetsov (ZK) equation, one can apply spectral renormalization/Petviashvilli's method [1, 11, 17]. However, these equations are semilinear, *i.e.* they are already of the form

$$-\nabla^2 u + \lambda u - f(u) = 0.$$

Thus, this popular approach is not immediately applicable to (5).

Another approach to solving for solitary wave profiles would be to use a shooting algorithm, though it is highly unstable, [6,33]. Other approaches are comparable to our sinc collocation approach: use finite differences or finite elements to construct a nonlinear algebraic system. The advantage of using sinc is that it naturally incorporates the boundary conditions at infinity, whereas one would need to introduce an artificial boundary condition for these problems.

It was necessary to extend ϕ_c from $(0, \infty)$ to be a function along the whole real axis to use sinc collocation. We accomplished this by an even extension. However, there are other possibilities, such as Laguerre polynomials, which naturally reside on the half line. These are summarized in [9]. The challenge to computing solitary wave solutions in higher dimensions is not particular to (3). There are similar difficulties with ZK and NLS. This method is likely to also prove effective in those problems.

Beyond methods for accurate computation of non-linear waves, these results provide the first critical tests for any code on magma dynamics. It should be stressed that the system (34) represents the most simplified version of magma dynamics that only includes the contributions of non-linear permeability and rheology to porosity evolution. More general systems are required to investigate the role of thermodynamics, chemistry, and the interaction with the large scale mantle flow. However, at their core, all of these problems need to reproduce the non-linear waves and the benchmarks presented here are a necessary and reasonably straightforward exercise in code verification. Moreover, these larger systems, still have the general quasi-static structure of the basic magma equations and require accurate and efficient multi-physics solvers for coupled hyperbolic/parabolic/elliptic systems. The physics based, block-preconditioners demonstrated here for magma may be a useful approach for more general problems.

Acknowledgements

This work has been supported by NSF Grants OCE-08-41079 and CMG-05-30853 and NSERC. The authors wish to thank M. I. Weinstein for comments throughout the development of the sinc approach. G. Simpson wishes to also thank M. Pugh for suggestions and C. Sulem for pointing out Sulem, Sulem & Frisch, [30], which was instrumental in identifying the strip of analyticity.

References

[1] M. J. Ablowitz and Z. H. Musslimani. Spectral renormalization method for computing self-localized solutions to nonlinear systems. *Optics letters*, 30(16):2140–2142, 2005.

[2] K. Al-Khaled. Sinc numerical solution for solitons and solitary waves. *Journal of Computational and Applied Mathematics*, 130(1-2):283–292, 2001.

[3] S. Balay, K. Buschelman, V. Eijkhout, W. D. Gropp, D. Kaushik, M. G. Knepley, L. C. McInnes, B. F. Smith, and H. Zhang. PETSc users manual. Technical Report ANL-95/11 - Revision 3.0.0, Argonne National Laboratory, 2008.

[4] S. Balay, K. Buschelman, W. D. Gropp, D. Kaushik, M. G. Knepley, L. C. McInnes, B. F. Smith, and H. Zhang. PETSc Web page, 2009. http://www.mcs.anl.gov/petsc.

[5] S. Balay, W. D. Gropp, L. C. McInnes, and B. F. Smith. Efficient management of parallelism in object oriented numerical software libraries. In E. Arge, A. M. Bruaset, and H. P. Langtangen, editors, *Modern Software Tools in Scientific Computing*, pages 163–202. Birkhäuser Press, 1997.

[6] V. Barcilon and O. Lovera. Solitary waves in magma dynamics. *Journal of Fluid Mechanics*, 204:121–133, 1989.

[7] V. Barcilon and F. Richter. Nonlinear waves in compacting media. *Journal of Fluid Mechanics*, 164:429–448, 1986.

[8] N. Bellomo. Nonlinear models and problems in applied sciences from differential quadrature to generalized collocation methods. *Math Comput Model*, 26(4):13–34, Jan 1997.

[9] J. Boyd. *Chebyshev and Fourier Spectral Methods*. Courier Dover Publications, 2001.

[10] R. Katz, M. G. Knepley, B. Smith, M. Spiegelman, and E. T. Coon. Numerical simulation of geodynamic processes using the Portable Extensible Toolkit for Scientific Computation. *Phys. Earth Planet. In.*, 163:52–68, 2007. doi:10.1016/j.pepi.2007.04.016.

[11] T. I. Lakoba and J. Yang. A generalized petviashvili iteration method for scalar and vector hamiltonian equations with arbitrary form of nonlinearity. *Journal of Computational Physics*, 226:1668, Oct 2007.

[12] J. Lund and K. Bowers. *Sinc Methods for Quadrature and Differential Equations*. Society for Industrial Mathematics, 1992.

[13] L. Lundin. A cardinal function method of solution of the equation $\delta u = u - u^3$. *Mathematics of Computation*, 35(151):747–756, 1980.

[14] J. L. Marzuola, S. Raynor, and G. Simpson. A system of odes for a perturbation of a minimal mass soliton. *Journal of Nonlinear Science*, 20(4):425–461, Jan 2010.

[15] D. McKenzie. The generation and compaction of partially molten rock. *Journal of Petrology*, 25(3):713–765, 1984.

[16] A. Mohsen and M. El-Gamel. On the Galerkin and collocation methods for two-point boundary value problems using sinc bases. *Computers and Mathematics with Applications*, 56(4):930–941, 2008.

[17] D. E. Pelinovsky and Y. Stepanyants. Convergence of petviashvili's iteration method for numerical approximation of stationary solutions of nonlinear wave equations. *SIAM Journal on Numerical Analysis*, 42(3):1110–1127, 2005.

[18] D. Scott and D. Stevenson. Magma solitons. *Geophysical Research Letters*, 11(11):1161–1161, 1984.

[19] D. Scott and D. Stevenson. Magma ascent by porous flow. *Journal of Geophysical Research*, 91:9283–9296, 1986.

[20] G. Simpson, M. Spiegelman, and M. Weinstein. Degenerate dispersive equations arising in the stuyd of magma dynamics. *Nonlinearity*, 20:21–49, 2007.

[21] G. Simpson and M. Weinstein. Asymptotic stability of ascending solitary magma waves. *SIAM Journal on Mathematical Analysis*, 40:1337–1391, 2008.

[22] G. Simpson, M. Weinstein, and P. Rosenau. On a hamiltonian pde arising in magma dynamics. *DCDS-B*, 10:903–924, 2008.

[23] M. Spiegelman. Flow in deformable porous media. part 1: Simple analysis. *Journal of Fluid Mechanics*, 247:17–38, 1993.

[24] M. Spiegelman. Flow in deformable porous media. part 2: Numerical analysis. *Journal of Fluid Mechanics*, 247:39–63, 1993.

[25] M. Spiegelman and R. Katz. A semi-lagrangian crank-nicolson algorithm for the numerical solution of advection-diffusion problems. *Geochem. Geophys. Geosyst.*, 7:Q04014, 2006. doi:10.1029/2005GC001073.

[26] A. Staniforth and J. Cote. Semi-Lagrangian integration schemes for atmospheric models—A review. *Mont. Weather Rev.*, 119(9):2206–2223, Sep 1991.

[27] F. Stenger. Numerical methods based on the whittaker cardinal, or sinc functions. *SIAM Review*, 23:165–224, 1981.

[28] F. Stenger. *Numerical Methods Based on Sinc and Analytic Functions*. Springer, 1993.

[29] F. Stenger. Summary of sinc numerical methods. *Journal of Computational and Applied Mathematics*, 121(1-2):379–420, 2000.

[30] C. Sulem, P. Sulem, and H. Frisch. Tracing complex singularities with spectral methods. *Journal of Computational Physics*, 50:138–161, 1983.

[31] J. Weideman and S. Reddy. A MATLAB differentiation matrix suite. *ACM Transactions on Mathematical Software (TOMS)*, 26(4):465–519, 2000.

[32] J. A. Whitehead and K. R. Helfrich. The korteweg-de vries equation from laboratory conduit and magma mibgration equations. *Geophysical Research Letters*, 13(6):545–546, 1986.

[33] C. Wiggins and M. Spiegelman. Magma migration and magmatic solitary waves in 3-D. *Geophysical Research Letters*, 22(10):1289–1292, 1995.

[34] V. E. Zakharov and E. A. Kuznetsov. Three-dimensional solitons. *Soviet Physics JETP*, 39:285, Aug 1974.

A Sinc Approximation

Here we briefly review sinc and its properties. The texts [12, 28] and the articles [8, 27, 29] provide an excellent overview. As noted, sinc collocation and Galerkin schemes have been used to solve a variety of partial differential equations.

A.1 Overview

Recall the definition of sinc,

$$\operatorname{sinc}(z) \equiv \begin{cases} \frac{\sin(\pi z)}{\pi z}, & \text{if } z \neq 0 \\ 1, & \text{if } z = 0. \end{cases}, \tag{41}$$

and for any $k \in \mathbb{Z}$, $h > 0$, let

$$S(k,h)(x) = \operatorname{sinc}\left(\frac{x - kh}{h}\right). \tag{42}$$

A sinc approximation is only appropriate for functions satisfying certain criteria. To define such functions we first define a *strip* about the real axis in the complex plane as

$$D_\nu = \{z \in \mathbb{C} \mid |\Im z| < \nu\}. \tag{43}$$

Defining the function space:

Definition A.1 *$B^p(D_\nu)$ is the set of analytic functions on D_ν satisfying:*

$$\|f(t + \mathrm{i}\cdot)\|_{L^1(-\nu,\nu)} = O(|t|^a), \quad \text{as } t \to \pm\infty, \text{ with } a \in [0,1), \tag{44a}$$

$$\lim_{y \to \nu^-} \|f(\cdot + \mathrm{i}y)\|_{L^p} + \lim_{y \to \nu^-} \|f(\cdot - \mathrm{i}y)\|_{L^p} < \infty. \tag{44b}$$

we have the following

Theorem A.2 (Theorem 2.16 of [12]) *Assume $f \in B^p(D_\nu)$, $p = 1, 2$, and f satisfies the decay estimate*

$$|f(x)| \leq C \exp(-\alpha|x|). \tag{45}$$

If h is selected such that

$$h = \sqrt{\pi\nu/(\alpha M)} \leq \min\left\{\pi\nu, \pi/\sqrt{2}\right\}, \tag{46}$$

then

$$\|\partial_x^n f - \partial_x^n C_M(f,h)\|_{L^\infty} \leq C M^{(n+1)/2} \exp\left((-\sqrt{\pi\nu\alpha M})\right).$$

This theorem justifies the sinc method, and guarantees rapid convergence for appropriate functions. Checking that a function satisfies all the hypotheses is non-trivial, and in practice it is omitted. However, it is essential to have a proper value of h to ensure convergence of algorithm; Theorem A.2 states the bound on h is related to estimates of both the decay rate and the domain of analyticity of the function.

A.2 Decay Rate

The decay rate is often easy to estimate. For the solitary waves solutions of (5), the asymptotically linear equation is

$$-c\phi_c' + n\phi_c' + c\left(\phi_c''' + \frac{d-1}{r}\phi_c'' - \frac{d-1}{r^2}\phi_c'\right) = 0$$

Integrating once,

$$-\frac{c-n}{c}(\phi_c - 1) + \phi_c'' + \frac{d-1}{r}\phi_c' = 0. \tag{47}$$

The solutions in dimensions $n = 1, 2, 3$ which decay as $r \to \infty$ are

$$\phi_c - 1 \propto \begin{cases} e^{-\sqrt{1-n/c}r} & n = 1, \\ k_0(\sqrt{1-n/c}r) & n = 2, \\ \frac{1}{r}e^{-\sqrt{1-n/c}r} & n = 3. \end{cases}$$

k_0 is a Bessel function, and it decays exponentially. Continuing to assume that (47) governs the large r behavior, the general decay relationship is

$$|\phi_c(r) - 1| \propto r^{-\frac{d-1}{2}} e^{-\sqrt{1-n/c}r} \tag{48}$$

The decay rate for Theorem A.2 is thus $\alpha = \sqrt{1-n/c}$.

A.3 Analyticity

The second parameter, ν, the distance into the complex plane which the function can be analytically continued off the real axis, is not as readily observed. Others have found $\nu = \pi/2$ sufficient. We use $\nu = \pi/2$ and can numerically confirm *a posteriori* that this is a reasonable value.

Checking this condition is equivalent to identifying the decay rate in Fourier space; ν satisfies

$$|\hat{u}(k)| \leq Ke^{-\nu|k|} \tag{49}$$

To see this, write $u(x)$ in terms of its Fourier Transform,

$$u(x) = \int_{-\infty}^{\infty} e^{ixk}\hat{u}(k)dk.$$

Evaluating u at $z = x + iy$,

$$u(z) = \int_{-\infty}^{\infty} e^{ixk}e^{-yk}\hat{u}(k)dk.$$

$u(z)$ is defined, provided

$$|u(z)| \leq \int_{-\infty}^{\infty} e^{-yk}|u(k)|dk < \infty$$

If $\hat{u}$ is bounded by $e^{-\nu|k|}$, then this integral is guaranteed to be finite for

$$-\nu < y < \nu$$

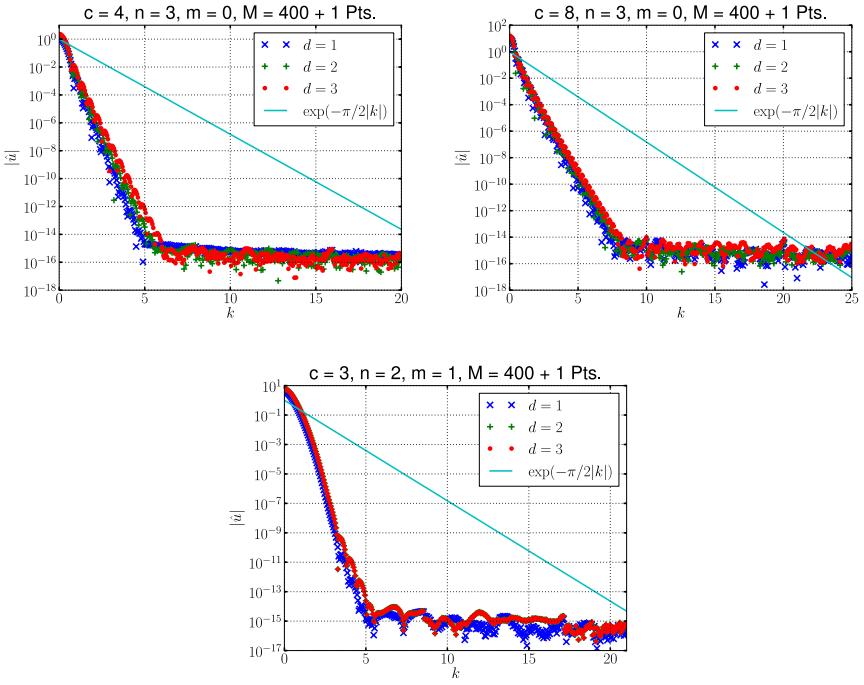

Figure 8: Fourier transforms of the solitary waves computed by the sinc algorithm.

Thus, we can compute the Fourier transform and assess its decay rate to identify ν. This was used in [30] to study the analyticity of the solutions to several partial differential equations.

Using our computed solitary waves, we approximate their Fourier transforms as follows. First, we form the even extension by reflection. Then we delete the node at x_{-M}; the solution now sits on $2M$ grid points. This extended solution is treated as periodic on $[x_{-M+1}, x_M]$ and its transform is computed. Figure 8 shows the resulting transforms. In these cases, we have resolved them to machine precision. More importantly, the solutions decay more rapidly than than $e^{-\pi/2|k|}$. This justifies using $\nu = \pi/2$. This value, together with $\alpha = \sqrt{1 - n/c}$, tells us that the largest value of h for which we can expect convergence is

$$h = \pi \sqrt{\frac{1}{2\gamma M}}, \quad \gamma = \sqrt{1 - n/c}$$

which is (15).

B Notes on Numerical Methods for solution of space-time PDE's

The algorithm demonstrated here uses second-order mixed Lagrange finite elements (P2-P2) in space for porosity and pressure and a second-order, semi-Lagrangian Crank-Nicolson scheme in time. The latter approach discretizes the generic hyperbolic advection-reaction PDE

$$\frac{Df}{Dt} = s(\mathbf{x}, t) \tag{50}$$

as a two level scheme via the trapezoidal rule

$$f(\mathbf{x}, t + \Delta t) = f(\mathbf{x}^*, t) + \frac{\Delta t}{2} \left[s(\mathbf{x}, t + \Delta t) + s(\mathbf{x}^*, t) \right] \tag{51}$$

where $\mathbf{x}^*$ is the take-off point of the characteristic that intersects point $\mathbf{x}$ at time $t + \Delta t$ [25, 26]. We use this scheme to approximate the strong form of equations (34) and then multiply by test functions and integrate to produce the non-linear weak form of the residual at time $t + \Delta t$ (Eq. (35)).

Semi-Lagrangian methods in finite elements can be considered a distortion and re-projection problem. For the pure advection problem, $Df/Dt = 0$, the weak-form becomes

$$\int_\Omega v f dx = \int_\Omega v f(\mathbf{x}^*) dx. \tag{52}$$

This is just the projection of the advected continuous function $f(\mathbf{x}^*, t)$ back onto the function space. To evaluate the RHS of Eq. (52) by quadrature, $f(\mathbf{x}^*)$ must be evaluated at the quadrature points. Therefore $\mathbf{x}^*$ should be the coordinates of the take-off points of the characteristics that intersect the quadrature point. This is different from finite difference problems where the characteristics intersect the grid points.

Given the weak form of the residual, it is straightforward to calculate the weak form of the Jacobian by functional differentiation. This exact Jacobian is assembled by FEniCS into a 2×2 non-symmetric block linear problem

$$\begin{bmatrix} A(f) & B(f,p) \\ \Delta t C(f) & D(f,p) \end{bmatrix} \begin{bmatrix} \delta p \\ \delta f \end{bmatrix} = - \begin{bmatrix} F_p \\ F_f \end{bmatrix} \tag{53}$$

where $\delta \mathbf{u} = [\delta p, \delta f]^T$ is the correction to the solution at each Newton step. Note if $\Delta t = 0$, the problem becomes linear. If we begin with an initial guess $f = f_0, p = 0$, then the problem reduces to solving

$$\begin{bmatrix} A(f_0) & B(f_0,p) \\ 0 & M \end{bmatrix} \begin{bmatrix} \delta p \\ \delta f \end{bmatrix} = - \begin{bmatrix} F_p(f_0) \\ 0 \end{bmatrix} \tag{54}$$

where M is the porosity mass matrix. Thus for $\Delta t = 0$, $\delta f = 0$ and $\delta p = -A(f_0)^{-1} F_p(f_0)$ which is just the discrete solution to (34b) for the pressure given porosity f_0.

For a non-zero time-step, we solve the linear problem, equation (53), using a block-preconditioned Newton-Krylov scheme implemented in PETSc, using their `FIELDSPLIT` block preconditioners[1]. Our preconditioner uses

$$P = \begin{bmatrix} A & 0 \\ \Delta t C & D \end{bmatrix} \tag{55}$$

as a lower triangular block pre-conditioner with one V-cycle of algebraic multi-grid on the A block and 2 sweeps of SOR on the D block, and then GMRES on the entire Jacobian. Other choices of preconditioners and solvers can be passed by command line arguments. However, we find this particular recipe to be robust and efficient in both 2 and 3-D, converging quadratically in two Newton steps with total residuals $||F(\mathbf{u})||_2 < 10^{-14}$ independent of dimension, grid-size, time-step and choice of model (n, m) or initial condition. Using the pre-conditioner as a solver, turns the algorithm into a Picard scheme with linear convergence (and a residual reduction of about an order of magnitude per non-linear step).

Given a high quality initial condition for porosity generated by the sinc-collocation scheme, we first project that solution onto our initial porosity as f_0, the general time stepping algorithm is:

Algorithm 1 SLCN-Newton-Krylov algorithm for Magma

Require: at $t = 0$, step $k = 0$: Set initial condition $f_k = f_0$, $p_k = 0$,
  set $\Delta t = 0$, Solve for p_k $(k = 0)$ by Newton
  set $\Delta t = dt$
  for $k = 1, 2, \ldots$ **do** {loop until $t \geq t_{max}$}
    Set initial Guess:
      set $p_k = p_{k-1}$
      solve $M f_k = \int q \left(g(\mathbf{x}^*) + \Delta t / 2 f_{k-1}^m p_k \right) dx$
    while $||F(\mathbf{u})||_2 >$ `tol` **do**
      Iterate preconditioned Newton-Krylov method for f_k,p_k
    end while
    $t \leftarrow t + \Delta t$
  end for

As with all non-linear solvers, having a good initial guess is critical to robustness. In the above algorithm we make a prediction for the porosity at the future time by solving Eq. (34a) as a projection problem with a lagged pressure field. M is the symmetric porosity mass matrix which can be solved with a few iterations of ICC preconditioned CG.

Though the above algorithm uses a constant time step, it is straightforward to implement adaptive time stepping in these two-level schemes for variable Δt.

[1] PETSc gives considerable flexibility for experimenting with a wide range of solvers and pre-conditioners